Rapid Communications

Solitary wave excitations of skyrmion strings in chiral magnets

Volodymyr P. Kravchuk,[1,2,3] Ulrich K. Rößler,[2] Jeroen van den Brink,[2,4,5] and Markus Garst[1,5,6]

[1]*Institut für Theoretische Festkörperphysik, Karlsruhe Institute of Technology, D-76131 Karlsruhe, Germany*

[2]*Leibniz-Institut für Festkörper- und Werkstoffforschung, IFW Dresden, D-01171 Dresden, Germany*

[3]*Bogolyubov Institute for Theoretical Physics of National Academy of Sciences of Ukraine, 03680 Kyiv, Ukraine*

[4]*Department of Physics, Washington University, St. Louis, Missouri 63130, USA*

[5]*Institut für Theoretische Physik, Technische Universität Dresden, D-01062 Dresden, Germany*

[6]*Institute for Quantum Materials and Technology, Karlsruhe Institute of Technology, D-76021 Karlsruhe, Germany*

(Received 21 February 2019; accepted 24 November 2020; published 17 December 2020)

Chiral magnets possess topological line excitations where the magnetization within each cross section forms a skyrmion texture. We study analytically and numerically the low-energy, nonlinear dynamics of such a skyrmion string in a field-polarized cubic chiral magnet, and we demonstrate that it supports solitary waves. These waves are in general nonreciprocal, i.e., their properties depend on the sign of their velocity v, but this nonreciprocity diminishes with decreasing $|v|$. An effective field-theoretical description of the solitary waves is derived that is valid in the limit $v \to 0$ and gives access to their profiles and their existence regime. Our analytical results are quantitatively confirmed with micromagnetic simulations for parameters appropriate for the chiral magnet FeGe. Similarities with solitary waves found in vortex filaments of fluids are pointed out.

DOI: 10.1103/PhysRevB.102.220408

Manifestations of one-dimensional topological objects can be found in diverse systems such as domain walls in magnetic films, vortex filaments in classical as well as quantum fluids, or cosmic strings in the universe [1,2]. Usually, these stringlike objects can elastically bend and twist, and this elasticity also determines their dynamical behavior at low energies. This results in collective low-amplitude excitations, for example, Kelvin waves [3] that propagate along vortex filaments and play a key role in the decay of superfluid turbulence [4]. Certain filaments can also support nonlinear solitary waves, which are spatially confined excitations that maintain a constant amplitude. For vortex filaments in fluids, solitary waves were theoretically predicted by Hasimoto [5] and subsequently observed experimentally [6].

Topological strings of a different kind arise in cubic chiral magnets such as MnSi, FeGe, or Cu_2OSeO_3. Here, the competition between exchange and Dzyaloshinskii-Moriya interactions stabilizes magnetic skyrmions, i.e., two-dimensional topological textures of the magnetization [7]. These skyrmions extend along the third direction forming topological strings. Skyrmion strings align with the applied magnetic field $\boldsymbol{H}$, and, under certain conditions, they condense into a hexagonal lattice forming a thermodynamically stable phase [8–10].

The nontrivial topology of two-dimensional skyrmion textures has direct consequences for their magnetization dynamics. It is reflected by their Thiele equation of motion that predicts an efficient coupling to spin currents with interesting spintronic applications [13,14] (for recent reviews, see Refs. [12,15–18]). It also leads to an emergent electrodynamics for electrons as well as spin waves, that scatter off skyrmions, resulting in topological Hall effects [19–23]. In addition, skyrmions possess characteristic internal degrees of freedom such as a breathing mode, that can be studied with magnetic resonance spectroscopy [24–30].

Even richer is the dynamics of three-dimensional skyrmion strings due to their additional degrees of freedom. Recently, it was demonstrated that spin waves generally propagate along these strings in a nonreciprocal fashion [31–33]. The elastic response of skyrmion strings gives rise to a nonreciprocal, nonlinear Hall effect [34,35]. Moreover, the merger of strings is necessarily accompanied with singular Bloch points that play the role of magnetic monopoles in the emergent electrodynamics [36–38]. In chiral magnets polarized either by a magnetic field or a uniaxial anisotropy, single skyrmion strings exist as topologically stable line excitations. Focusing on cubic chiral magnets, we demonstrate in the present Rapid Communication that solitary waves can propagate along such isolated strings (see Fig. 1), efficiently transmitting energy, linear, and angular momentum.

When damping is neglected, the magnetization dynamics is described by the Landau-Lifshitz equation $\partial_t \boldsymbol{n} = -\gamma(\boldsymbol{n} \times \boldsymbol{B}_{\rm eff})$ for the orientation of the magnetization represented by the unit vector $\boldsymbol{n}$ where $\gamma = g\mu_B/\hbar$ is the gyromagnetic ratio. The effective magnetic field, $\boldsymbol{B}_{\rm eff} = -\frac{1}{M_s}\frac{\delta V}{\delta \boldsymbol{n}}$, derives from the potential $V = \int d\boldsymbol{r}\, \mathcal{V}$; for cubic chiral magnets the potential density is given by

$$\mathcal{V}(\boldsymbol{n}, \partial_i \boldsymbol{n}) = A(\partial_i \boldsymbol{n})^2 + D\boldsymbol{n}(\nabla \times \boldsymbol{n}) - \mu_0 M_s H n_z, \qquad (1)$$

with the exchange stiffness A, the Dzyaloshinskii-Moriya interaction D, the magnetic constant μ_0, the saturation magnetization M_s, and the magnetic field $\boldsymbol{H} = \hat{\boldsymbol{z}}H$ that defines the z axis. Dipolar interactions are neglected for

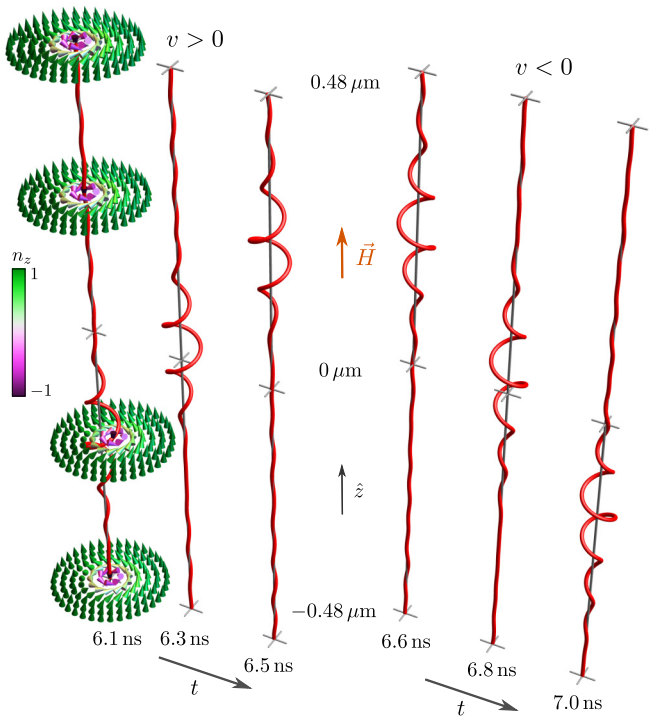

FIG. 1. Solitary wave excitation of an isolated skyrmion string, that is aligned with the magnetic field $\boldsymbol{H} = \hat{z}H$, propagating in a direction parallel ($v > 0$) and antiparallel ($v < 0$) to $\boldsymbol{H}$. The figure is produced by micromagnetic simulation with parameters $\omega_{c2}/(2\pi) = 10.4$ GHz and $2\pi/Q = 70$ nm typical for the chiral magnet FeGe [11,12]. The dimensionless field is $h = 2.16$ corresponding to $\mu_0 H \approx 0.8$ T for $g \approx 2$ resulting in a skyrmion string radius of approximately 5 nm. Solitary waves with amplitude $R_0 \approx 5.8$ nm are created at time $t = 0$ and propagate with velocity $|v| \approx 1$ km/s. Periodic boundary conditions are employed, and the red line is defined according to Eq. (2). Lengths in the (x, y) plane are upscaled by a factor of 5 for visualization.

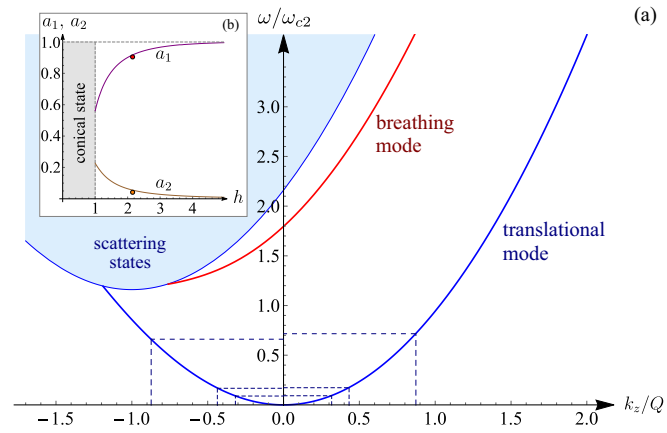

FIG. 2. (a) Linear spin-wave spectrum of a skyrmion string for wave vectors k_z along the string and an applied magnetic field $h = 2.16$. The spectrum of the low-energy translational mode has the form $\omega(k_z)/\omega_{c2} \approx a_1(k_z/Q)^2 + a_2(k_z/Q)^3 + \cdots$ for small k_z. The nonreciprocity due to a_2 is small for wave vectors $|k_z| \ll k^*$ where $k^* = a_1 Q/a_2$ ($k^*/Q = 22.02$ for $h = 2.16$). (b) Field dependence of the parameters a_1 and a_2. The dashed lines in (a) as well as the points marked in (b) refer to Figs. 3 and 4.

simplicity. The scales for frequency and wave vectors are given by $\omega_{c2} = \gamma D^2/(2AM_s)$ and $Q = D/(2A)$, respectively, and the theory (1) only depends on a single dimensionless parameter $h = \gamma\mu_0 H/\omega_{c2}$ parametrizing the strength of the magnetic field.

For $h > 1$, the ground state of the theory (1) is field polarized, $n_z = 1$, and we focus on this parameter regime in the following. This field-polarized state possesses a static skyrmion string excitation aligned with the field $\boldsymbol{H}$ [39]. This is a smooth magnetic texture with a quantized topological charge $\mathcal{N}_{\text{top}} = \int dxdy\, \rho_{\text{top}} = -1$ for all values of z, i.e., for each cross section perpendicular to $\boldsymbol{H}$. Here, $\rho_{\text{top}}(\boldsymbol{r}) = \frac{1}{4\pi}\boldsymbol{n}(\partial_x \boldsymbol{n} \times \partial_y \boldsymbol{n})$ is the topological charge density within the (x, y) plane.

We first discuss the dynamical excitations of the skyrmion string on the level of linear spin-wave theory. The excitation spectrum of the skyrmion was studied analytically in Refs. [28,29]. Extending this analysis to the skyrmion string, one obtains the spectrum as a function of wave vector k_z along the field [32]—see Fig. 2 and the Supplemental Material [40] for details (see also Refs. [41–51] therein). The spectrum lacks mirror symmetry with respect to k_z, i.e., it is nonreciprocal due to the Dzyaloshinskii-Moriya interaction. The shaded region contains the scattering states, that are gapped for any $h > 1$. In addition, there are magnon-skyrmion bound states with wave functions localized to the skyrmion string. For the range of k_z shown in Fig. 2, there exist two dispersive bound states: the breathing mode, that possesses a finite energy at $k_z = 0$, and the translational Goldstone mode. The spectrum of the latter is gapless, $\omega(k_z) \propto k_z^2$ for $|k_z| \ll k^*$, due to the translational invariance of the theory (1) [52]; for the definition of k^*, see Fig. 2.

The degree of freedom associated with the Goldstone mode is the linear momentum of the skyrmion texture within the (x, y) plane. This linear momentum corresponds to a collective coordinate $\boldsymbol{R} = X\hat{\boldsymbol{x}} + Y\hat{\boldsymbol{y}}$, and it is given by the first moment of the topological charge density [28,29,53],

$$\boldsymbol{R}(z, t) = \frac{1}{\mathcal{N}_{\text{top}}} \int dxdy(x\hat{\boldsymbol{x}} + y\hat{\boldsymbol{y}})\rho_{\text{top}}(\boldsymbol{r}, t). \tag{2}$$

We demand that the skyrmion string does not bend back so that its linear momentum is uniquely defined for each value of z. The dynamics of $\boldsymbol{R}$ is governed by the Thiele equation [13] that reads in the absence of damping $\boldsymbol{G} \times \partial_t \boldsymbol{R} = \boldsymbol{F}$. The gyrocoupling vector $\boldsymbol{G} = \hat{z}4\pi\mathcal{N}_{\text{top}} M_s/\gamma$ is proportional to the topological charge $\mathcal{N}_{\text{top}}$, and $\boldsymbol{F}$ is a force that acts on the string [40].

In the following, we limit ourselves to the low-energy limit where the force, in the absence of external forces, is expected to be generated by the skyrmion string itself, $\boldsymbol{F} = -\frac{\delta V_{\text{eff}}}{\delta \boldsymbol{R}}$. The effective potential $V_{\text{eff}} = \int dz \mathcal{V}_{\text{eff}}$ with a local density $\mathcal{V}_{\text{eff}}$ can be phenomenologically constructed using symmetry considerations. Due to translational invariance $\mathcal{V}_{\text{eff}}$ cannot depend on $\boldsymbol{R}$ itself but only on its derivatives with respect to z, i.e., $\partial_z \boldsymbol{R}$, $\partial_z^2 \boldsymbol{R}$, etc. We will limit ourselves to the case of small $|\partial_z^2 \boldsymbol{R}|/|\partial_z \boldsymbol{R}| \ll k^*$ so that second- and higher-order derivatives can be omitted. Moreover, due to invariance of

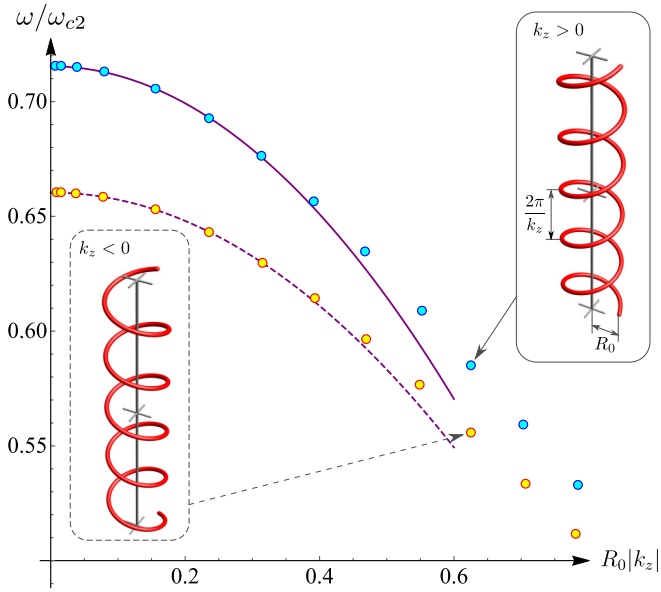

FIG. 3. Nonlinear spin waves of the skyrmion string studied with micromagnetic simulations for $h = 2.16$. The energies of low-energy waves, $X + iY = R_0 e^{ik_z z - i\omega t}$, with fixed wave vector $k_z = 0.87Q$ but for various amplitudes R_0 between 0.1 and 10 nm are fitted to $\omega/\omega_{c2} = a_1(k_z/Q)^2 + a_2(k_z/Q)^3 - (k_z R_0)^2[b_1(k_z/Q)^2 + b_2(k_z/Q)^3]$, and we obtain $a_1 \approx 0.903$, $a_2 \approx 0.041$, $b_1 \approx 0.467$, $b_2 \approx 0.071$. The values for a_1 and a_2 are in good agreement with linear spin-wave theory [see dots in the inset of Fig. 2(b)]. The coefficients a_2 and b_2 account for the leading nonreciprocal corrections, that are small for $|k_z| \ll k^*$ and are omitted in Eq. (4). The amplitude for both simulation snapshots shown in the insets is $R_0 = 8$ nm where lengths in the (x, y) plane are upscaled by a factor of 5.

the theory (1) with respect to combined rotations of real and spin space around the z axis, the effective potential is only a function of $(\partial_z \boldsymbol{R})^2$. Assuming analyticity, we can approximate the potential for small $(\partial_z \boldsymbol{R})^2$ by its Taylor expansion, and we obtain $\mathcal{V}_{\text{eff}} \approx \frac{1}{2}K_1(\partial_z \boldsymbol{R})^2 - \frac{1}{4}K_2(\partial_z \boldsymbol{R})^4$.

The elastic coefficient K_1 quantifies the stiffness of the string, and it is positive in order to guarantee stability. Importantly, the leading-order nonlinearity possesses a coefficient $K_2 > 0$. In the framework of nonlinear spin-wave theory, this nonlinearity arises from fluctuations of the stiffness K_1 that, in second-order perturbation theory, gives rise to a positive K_2. Here, we determine both $K_1 = a_1|\boldsymbol{G}|\omega_{c2}/Q^2$ and $K_2 = b_1|\boldsymbol{G}|\omega_{c2}/Q^2$ numerically with the help of micromagnetic simulations of nonlinear spin waves (see Fig. 3). For a magnetic field $h = 2.16$ we obtain $a_1 \approx 0.903$ and $b_1 \approx 0.467$.

In the following, it is convenient to introduce the dimensionless wave function

$$\psi = \sqrt{\frac{2b_1}{a_1}} Q(X + iY). \tag{3}$$

Using dimensionless time, $x_0 = 2a_1 t\omega_{c2}$, and length, $x_1 = zQ$, the Thiele equation reduces to the Euler-Lagrange equation for the Lagrange density,

$$\mathcal{L} = \frac{i}{2}(\psi^*\partial_0\psi - \psi\partial_0\psi^*) - \frac{1}{2}|\partial_1\psi|^2 + \frac{1}{8}|\partial_1\psi|^4. \tag{4}$$

We arrive at the result that the low-energy dynamics of the skyrmion string is described by a nonlinear Schrödinger equation with an attractive interaction $|\partial_1\psi|^4$ involving the derivative of the wave function.

Now, we demonstrate that the theory (4) possesses solitary waves, and its elementary conservation laws are sufficient to derive their properties. The particle density $j_0 = |\psi|^2$ obeys the conservation law $\partial_\mu j_\mu = 0$ with the associated current j_1 along the z axis. The density $|\psi|^2 \propto \boldsymbol{R}^2$ is in fact proportional to the angular momentum of the skyrmion within the (x, y) plane [28,53] so that the total density measures the total angular momentum of the string $J_z \propto \int dx_1 |\psi|^2$. In addition, the energy-momentum tensor is conserved, $\partial_\mu T_{\mu\nu} = 0$ [40].

We look for solitary wave solutions,

$$\psi(x_\mu) = \Psi(x_1 - vx_0)e^{i[v(x_1 - vx_0) + \frac{v^2}{2}x_0]}e^{-i\omega x_0}, \tag{5}$$

that can be expressed as the Galilean transform of a wave function Ψ oscillating with frequency ω. As the interaction $|\partial_1\psi|^4$ breaks Galilean invariance, we expect that the function Ψ will depend on the velocity v. The conserved densities reduce for Eq. (5) to functions of the variable $\xi \equiv x_1 - vx_0$ only, so that $\mathcal{T}_v \equiv -vT_{0v} + T_{1v}$ as well as $\mathcal{J} \equiv -vj_0 + j_1$ become independent of both space and time. In fact, the three constants are linearly dependent as one finds $\mathcal{T}_0 = (\omega - \frac{v^2}{2})\mathcal{J} - v\mathcal{T}_1$.

Moreover, for a localized solitary wave with boundary conditions $|\Psi(\xi)| \to 0$ for $\xi \to \pm\infty$ these constants vanish, $\mathcal{T}_v = 0$. Decomposing $\Psi(\xi) = A(\xi)e^{i\phi(\xi)}$ into magnitude and phase we can solve these two equations for A and its derivative A'. Remarkably, we find that they are simply parametrized by the derivative of the phase, $\phi' = \partial_\xi\phi$,

$$A(\xi) = \frac{1}{|v|\sqrt{1+\alpha}} f_1\left(\frac{\phi'(\xi)}{v}\right), \tag{6a}$$

$$A'(\xi) = \pm\frac{1}{\sqrt{1+\alpha}} f_2\left(\frac{\phi'(\xi)}{v}, \alpha\right), \tag{6b}$$

where $\alpha \equiv -2\omega/v^2$ represents the frequency. The two functions are $f_1(p) = \sqrt{p(2-p)}/(1+p)$ and $f_2(p,\alpha) = \sqrt{p(2\alpha - p + p^2)}/\sqrt{1+p}$. A closed curve in the (A, A') plane, that converges to the origin for $|\xi| \to \infty$, is obtained for $0 < \alpha < \frac{1}{8}$. This constraint yields a two-parameter family of solitary wave solutions parametrized by α and the velocity v (see Ref. [40] for details).

Taking the derivative of Eq. (6a) and comparing with Eq. (6b) yields a first-order ordinary differential equation for ϕ', that is easily solved. One obtains a wave function where both derivative ϕ' and magnitude A are locally confined (see Fig. 4). Their extremal values are

$$\phi'_{\max} = \frac{v}{2}(1 - \sqrt{1 - 8\alpha}), \tag{7a}$$

$$A_{\max} = \frac{\sqrt{2}}{|v|}\frac{\sqrt{4\alpha + 1 - \sqrt{1-8\alpha}}}{\sqrt{1+\alpha}(3 - \sqrt{1-8\alpha})}, \tag{7b}$$

and both vanish for $\alpha \to 0^+$. For small α we can approximate $f_1(p) \approx \sqrt{2p}$ and $f_2(p,\alpha) \approx \sqrt{p(2\alpha - p)}$, and we obtain ex-

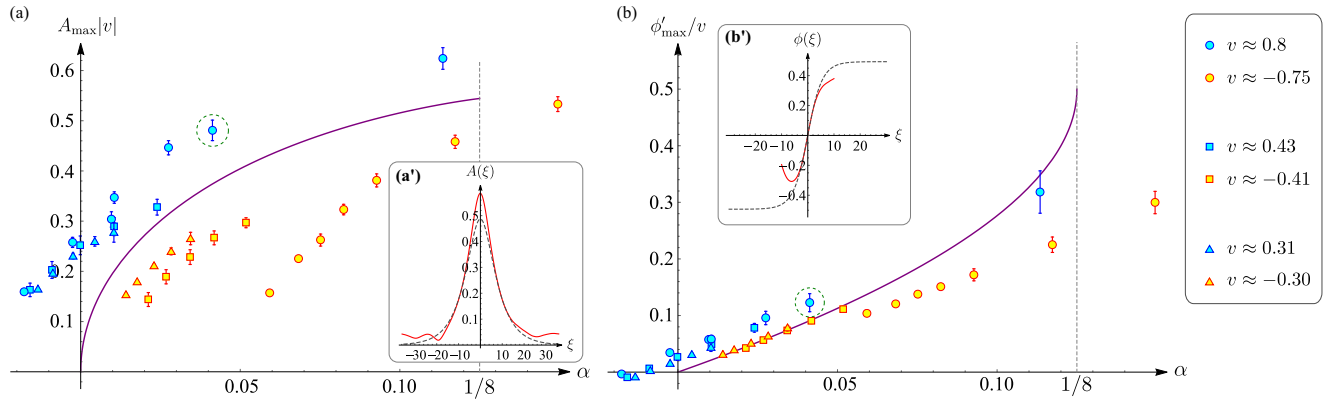

FIG. 4. Profile parameters of solitary waves extracted from micromagnetic simulations at $h = 2.16$ (symbols) for various values of dimensionless velocity v (in units of 1310 m/s). The profiles generally depend on the sign of v, but this nonreciprocity decreases with decreasing $|v|$ and the profiles approach the analytical predictions of Eq. (7) (lines) valid for $v \to 0$. The insets show a full numerical profile (red lines) for $\alpha \approx 0.04$ (marked by dashed circles in the main panels) with a comparison to the solution of Eq. (6) (dashed lines).

plicitly the profile for a solitary wave centered at $\xi = 0$,

$$\phi(\xi) \approx 2\sqrt{\alpha}\tanh(\sqrt{\alpha}v\xi), \quad A(\xi) \approx \frac{2}{|v|}\frac{\sqrt{\alpha}}{\cosh(\sqrt{\alpha}v\xi)}, \quad (8)$$

up to a constant phase shift. From these expressions we can read off the spatial width $\xi_w \sim \frac{1}{|v|\sqrt{\alpha}}$ that diverges in this limit.

Note that the amplitude $A_{\max}$ in Eq. (7b) diverges for small velocities v but this does not invalidate the theory. The Taylor expansion of the effective potential $\mathcal{V}_{\text{eff}}$ is controlled as long as the derivative $|\partial_z \boldsymbol{R}| \propto |\partial_1 \psi|$ remains small. Its maximal value is attained at the center of the solitary wave, that is, small $|\partial_1\psi|^2|_{\max} \sim \alpha$, for $\alpha \to 0^+$. Moreover, nonreciprocal corrections associated with the second derivative $|\partial_1^2\psi|/|\partial_1\psi| \sim v$ are negligible as long as the velocity is small, and, therefore, the theory (4) is under control for small v and α. As shown in Ref. [40], the lifetime of the solitary wave due to a finite Gilbert damping is also large in this limit, $\tau \sim 1/v^2$. We note that nonreciprocal corrections can, in principle, be taken into account, spoiling, however, the simplicity of Eqs. (6).

The solitary wave carries energy, linear, and angular momentum along the string. In the limit of small α, the total energy is on the order $E \sim \frac{\sqrt{\alpha}}{|v|}$, and it diverges for small velocities due to the large width of the wave, $\xi_w \sim \frac{1}{|v|\sqrt{\alpha}}$. The energy density, however, remains small, $E/\xi_w \sim \alpha$. For the total linear and angular momentum we obtain, respectively, $P \sim \frac{\sqrt{\alpha}}{|v|v}$ and $J_z \sim \frac{\sqrt{\alpha}}{v^3}$. Both are even more singular than E due to the large amplitude [Eq. (7b)]. As discussed above, the corresponding total currents are obtained by multiplying with v.

Our micromagnetic simulations confirm the presence of stable solitary waves (see Fig. 1). We have extracted numerically their profiles for various values of v and α (see Fig. 4 and Ref. [40]). The profiles are found to be nonreciprocal, i.e., they depend on the sign of the velocity v. This nonreciprocity, however, decreases with decreasing $|v|$, and we find that they approach for $v \to 0$ the analytical predictions for this limit. As the width as well as the amplitude of the solitary wave diverges for $v \to 0$, finite-size effects of our simulation hamper the study of velocities smaller than the values listed in Fig. 4. Solitary waves are confirmed to exist for α within the full range between zero and 1/8. For larger α, the skyrmion string becomes unstable and breaks, at least, for the discretization used in our micromagnetic simulation.

Finally, we compare with the dynamics of vortex filaments in superfluids. Vortices are singular defects of the superfluid order parameter in contrast to skyrmions that are smooth textures. As a consequence, the dynamics of vortex filaments are in general governed by a nonlocal Biot-Savart law. This nonlocality is at the origin of the nonanalytic dispersion, $\omega(k_z) \sim k_z^2 \log k_z$, of Kelvin waves and it leads to stretching instabilities such as the development of hairpins in the filament [2].

Only when this nonlocality is neglected within the localized induction approximation (LIA), is the dynamics of the vortex filament also described by a local Schrödinger equation with a Hamiltonian proportional to its length, $H = \int dx_1 \mathcal{H}$ with $\mathcal{H} = \sqrt{1 + |\partial_1\psi|^2}$ [4]. As a consequence, its length is conserved and stretching is neglected within the LIA. Interestingly, the resulting Schrödinger equation is integrable [54] and its solitons were first discussed by Hasimoto [5]. In the limit of small intrinsic curvature κ of the filament, $|\partial_1\psi|$ remains small and after Taylor expanding $\mathcal{H}$ the theory approximately coincides with that of Eq. (4) [55]. Hasimoto's soliton solution indeed reduces to Eq. (8) in this limit.

This has interesting consequences for the solitary waves studied here. Whereas the theory (4) itself is claimed to be nonintegrable [55], it is very close to an integrable theory in the limit of its applicability. This implies that the solitary waves of the skyrmion string are expected to be approximate solitons that almost retain their shape in collisions. Using the solitary waves as carriers, the skyrmion string therefore serves as a transmission line that allows for the simultaneous, though nonreciprocal, information transfer in both directions. Experimentally, solitary waves could be created, e.g., by inhomogeneous spin-transfer torques [12].

M.G. was supported by DFG SFB1143 (Project A07, Project-id. 247310070), and DFG Project-id. 270344603 and 324327023. J.v.d.B is supported by SFB1143, Project A05.

We acknowledge support from the UKRATOP project funded by the German Federal Ministry of Education and Research, Grant No. 01DK18002. In part, the work of V.P.K. was supported by the Program of Fundamental Research of the Department of Physics and Astronomy of the National Academy of Sciences of Ukraine (Project No. 0120U100855). We thank D. Sheka and Y. Gaididei for fruitful discussions, and U. Nitzsche for technical support.

[1] A. P. Malozemoff and J. C. Slonzewski, *Magnetic Domain Walls in Bubble Materials* (Academic, New York, 1979).
[2] L. M. Pismen, in *Vortices in Nonlinear Fields*, edited by J. Birman (Oxford University Press, Oxford, UK, 1999).
[3] W. Thomson, Philos. Mag. **10**, 155 (1880).
[4] B. V. Svistunov, Phys. Rev. B **52**, 3647 (1995).
[5] H. Hasimoto, J. Fluid Mech. **51**, 477 (1972).
[6] E. J. Hopfinger and F. K. Browand, Nature (London) **295**, 393 (1982).
[7] A. N. Bogdanov and D. A. Yablonskiĭ, Zh. Eksp. Teor. Fiz. **95**, 178 (1989) [Sov. Phys. JETP **68**, 101 (1989)].
[8] S. Mühlbauer, B. Binz, F. Jonietz, C. Pfleiderer, A. Rosch, A. Neubauer, R. Georgii, and P. Böni, Science **323**, 915 (2009).
[9] S. Seki, X. Z. Yu, S. Ishiwata, and Y. Tokura, Science **336**, 198 (2012).
[10] A. Bauer and C. Pfleiderer, in *Topological Structures in Ferroic Materials: Domain Walls, Vortices and Skyrmions*, edited by J. Seidel (Springer, Berlin, 2016).
[11] S. Haraldson, L. Pettersson, and S. M. Bhagat, J. Magn. Reson. **32**, 115 (1978).
[12] N. Nagaosa and Y. Tokura, Nat. Nanotechnol. **8**, 899 (2013).
[13] A. A. Thiele, Phys. Rev. Lett. **30**, 230 (1973).
[14] F. Jonietz, S. Mühlbauer, C. Pfleiderer, A. Neubauer, W. Münzer, A. Bauer, T. Adams, R. Georgii, P. Böni, R. A. Duine, K. Everschor, M. Garst, and A. Rosch, Science **330**, 1648 (2010).
[15] R. Wiesendanger, Nat. Rev. Mater. **1**, 16044 (2016).
[16] A. Fert, N. Reyren, and V. Cros, Nat. Rev. Mater. **2**, 17031 (2017).
[17] W. Jiang, G. Chen, K. Liu, J. Zang, S. G. te Velthuis, and A. Hoffmann, Phys. Rep. **704**, 1 (2017).
[18] K. Everschor-Sitte, J. Masell, R. M. Reeve, and M. Kläui, J. Appl. Phys. **124**, 240901 (2018).
[19] A. Neubauer, C. Pfleiderer, B. Binz, A. Rosch, R. Ritz, P. G. Niklowitz, and P. Böni, Phys. Rev. Lett. **102**, 186602 (2009).
[20] M. Lee, W. Kang, Y. Onose, Y. Tokura, and N. P. Ong, Phys. Rev. Lett. **102**, 186601 (2009).
[21] T. Schulz, R. Ritz, A. Bauer, M. Halder, M. Wagner, C. Franz, C. Pfleiderer, K. Everschor, M. Garst, and A. Rosch, Nat. Phys. **8**, 301 (2012).
[22] J. Iwasaki, A. J. Beekman, and N. Nagaosa, Phys. Rev. B **89**, 064412 (2014).
[23] M. Mochizuki, X. Z. Yu, S. Seki, N. Kanazawa, W. Koshibae, J. Zang, M. Mostovoy, Y. Tokura, and N. Nagaosa, Nat. Mater. **13**, 241 (2014).
[24] M. Mochizuki, Phys. Rev. Lett. **108**, 017601 (2012).
[25] Y. Onose, Y. Okamura, S. Seki, S. Ishiwata, and Y. Tokura, Phys. Rev. Lett. **109**, 037603 (2012).
[26] T. Schwarze, J. Waizner, M. Garst, A. Bauer, I. Stasinopoulos, H. Berger, C. Pfleiderer, and D. Grundler, Nat. Mater. **14**, 478 (2015).
[27] S.-Z. Lin, C. D. Batista, and A. Saxena, Phys. Rev. B **89**, 024415 (2014).
[28] C. Schütte and M. Garst, Phys. Rev. B **90**, 094423 (2014).
[29] V. P. Kravchuk, D. D. Sheka, U. K. Rößler, J. van den Brink, and Y. Gaididei, Phys. Rev. B **97**, 064403 (2018).
[30] M. Garst, J. Waizner, and D. Grundler, J. Phys. D: Appl. Phys. **50**, 293002 (2017).
[31] X. Xing, Y. Zhou, and H. B. Braun, Phys. Rev. Appl. **13**, 034051 (2020).
[32] S.-Z. Lin, J.-X. Zhu, and A. Saxena, Phys. Rev. B **99**, 140408(R) (2019).
[33] S. Seki, M. Garst, J. Waizner, R. Takagi, N. D. Khanh, Y. Okamura, K. Kondou, F. Kagawa, Y. Otani, and Y. Tokura, Nat. Commun. **11**, 256 (2020).
[34] S. Mühlbauer, J. Kindervater, T. Adams, A. Bauer, U. Keiderling, and C. Pfleiderer, New J. Phys. **18**, 075017 (2016).
[35] T. Yokouchi, S. Hoshino, N. Kanazawa, A. Kikkawa, D. Morikawa, K. Shibata, T. Arima, Y. Taguchi, F. Kagawa, N. Nagaosa, and Y. Tokura, Sci. Adv. **4**, eaat1115 (2018).
[36] P. Milde, D. Köhler, J. Seidel, L. M. Eng, A. Bauer, A. Chacon, J. Kindervater, S. Mühlbauer, C. Pfleiderer, S. Buhrandt, C. Schütte, and A. Rosch, Science **340**, 1076 (2013).
[37] C. Schütte and A. Rosch, Phys. Rev. B **90**, 174432 (2014).
[38] S.-Z. Lin and A. Saxena, Phys. Rev. B **93**, 060401(R) (2016).
[39] A. Bogdanov and A. Hubert, J. Magn. Magn. Mater **138**, 255 (1994).
[40] See Supplemental Material at http://link.aps.org/supplemental/10.1103/PhysRevB.102.220408 for details of the linear spin wave calculation, the solution for the solitary wave, and the micromagnetic simulations as well as for various movies illustrating the solitary wave dynamics.
[41] B. A. Ivanov, A. K. Kolezhuk, and G. M. Wysin, Phys. Rev. Lett. **76**, 511 (1996).
[42] B. A. Ivanov, V. M. Murav'ev, and D. D. Sheka, JETP **89**, 583 (1999).
[43] D. D. Sheka, B. A. Ivanov, and F. G. Mertens, Phys. Rev. B **64**, 024432 (2001).
[44] G. Peano, Math. Ann. **37**, 182 (1890).
[45] M. Donahue and D. Porter, OOMMF User's Guide, Version 1.0, Interagency Report No. NISTIR 6376 (National Institute of Standards and Technology, Gaithersburg, MD, 1999). We used the 3D version of the 2.0α0 release.
[46] D. Cortés-Ortuño, M. Beg, V. Nehruji, R. A. Pepper, and H. Fangohr, OOMMF extension: Dzyaloshinskii-Moriya interaction (DMI) for crystallographic classes T and O (Version 1.0), Zenodo, http://doi.org/10.5281/zenodo.1196820 (2018).
[47] M. Beg, R. Carey, W. Wang, D. Cortés-Ortuño, M. Vousden, M.-A. Bisotti, M. Albert, D. Chernyshenko, O. Hovorka, R. L. Stamps, and H. Fangohr, Sci. Rep. **5**, 17137 (2015).

[48] S. Rohart and A. Thiaville, Phys. Rev. B **88**, 184422 (2013).

[49] S. L. Zhang, I. Stasinopoulos, T. Lancaster, F. Xiao, A. Bauer, F. Rucker, A. A. Baker, A. I. Figueroa, Z. Salman, F. L. Pratt, S. J. Blundell, T. Prokscha, A. Suter, J. Waizner, M. Garst, D. Grundler, G. van der Laan, C. Pfleiderer, and T. Hesjedal, Sci. Rep. **7**, 123 (2017).

[50] A. Vansteenkiste, K. W. Chou, M. Weigand, M. Curcic, V. Sackmann, H. Stoll, T. Tyliszczak, G. Woltersdorf, C. H. Back, G. Schutz, and B. Van Waeyenberge, Nat. Phys. **5**, 332 (2009).

[51] I. Stasinopoulos, S. Weichselbaumer, A. Bauer, J. Waizner, H. Berger, S. Maendl, M. Garst, C. Pfleiderer, and D. Grundler, Appl. Phys. Lett. **111**, 032408 (2017).

[52] M. Kobayashi and M. Nitta, Phys. Rev. D **90**, 025010 (2014).

[53] N. Papanicolaou and T. N. Tomaras, Nucl. Phys. B **360**, 425 (1991).

[54] K. Konno and Y. H. Ichikawa, Chaos, Solitons Fractals **2**, 237 (1992).

[55] G. Boffetta, A. Celani, D. Dezzani, J. Laurie, and S. Nazarenko, J. Low Temp. Phys. **156**, 193 (2009).